HAL
open science

High magnetic field ultrasound study of spin freezing in La_1.88Sr_0.12CuO_4

Shang-Fei Wu, Marc-Henri Julien, Mehdi Frachet, Siham Benhabib, Igor Vinograd, Baptiste Vignolle, Hadrien Mayaffre, Steffen Krämer, Tohru Kurosawa, Cyril Proust, et al.

To cite this version:

Shang-Fei Wu, Marc-Henri Julien, Mehdi Frachet, Siham Benhabib, Igor Vinograd, et al.. High magnetic field ultrasound study of spin freezing in La_1.88Sr_0.12CuO_4. Physical Review B, 2021, 103 (11), 115133 (11 p.). 10.1103/PhysRevB.103.115133 . hal-03060546

HAL Id: hal-03060546

https://hal.science/hal-03060546v1

Submitted on 14 Dec 2020

HAL is a multi-disciplinary open access archive for the deposit and dissemination of scientific research documents, whether they are published or not. The documents may come from teaching and research institutions in France or abroad, or from public or private research centers.

L'archive ouverte pluridisciplinaire **HAL**, est destinée au dépôt et à la diffusion de documents scientifiques de niveau recherche, publiés ou non, émanant des établissements d'enseignement et de recherche français ou étrangers, des laboratoires publics ou privés.

arXiv:2011.00562v1 [cond-mat.supr-con] 1 Nov 2020

High magnetic field ultrasound study of spin freezing in $La_{1.88}Sr_{0.12}CuO_4$

M. Frachet,[1,*] S. Benhabib,[1] I. Vinograd,[1] S.-F. Wu,[1] B. Vignolle,[2] H. Mayaffre,[1] S. Krämer,[1] T. Kurosawa,[3] N. Momono,[4] M. Oda,[3] J. Chang,[5] C. Proust,[1] M.-H. Julien,[1] and D. LeBoeuf[1,†]

[1] *Univ. Grenoble Alpes, INSA Toulouse, Univ. Toulouse Paul Sabatier, EMFL, CNRS, LNCMI, 38000, Grenoble, France*
[2] *Institut de Chimie de la Matière Condensée, Bordeaux, France*
[3] *Department of Physics, Hokkaido University, Sapporo 060-0810, Japan*
[4] *Muroran Institute of Technology, Muroran 050-8585, Japan*
[5] *Department of Physics, University of Zurich, CH-8057 Zurich, Switzerland*

(Dated: November 3, 2020)

High-T_c cuprate superconductors host spin, charge and lattice instabilities. In particular, in the antiferromagnetic glass phase, over a large doping range, lanthanum based cuprates display a glass-like spin freezing with antiferromagnetic correlations. Previously, sound velocity anomalies in $La_{2-x}Sr_xCuO_4$ (LSCO) for hole doping $p \geq 0.145$ were reported and interpreted as arising from a coupling of the lattice to the magnetic glass [Frachet, Vinograd *et al.*, Nat. Phys. **16**, 1064-1068 (2020)]. Here we report both sound velocity and attenuation in LSCO $p = 0.12$, *i.e.* at a doping level for which the spin freezing temperature is the highest. Using high magnetic fields and comparing with nuclear magnetic resonance (NMR) measurements, we confirm that the anomalies in the low temperature ultrasound properties of LSCO are produced by a coupling between the lattice and the spin glass. Moreover, we show that both sound velocity and attenuation can be simultaneously accounted for by a simple phenomenological model originally developed for canonical spin glasses. Our results point towards a strong competition between superconductivity and spin freezing, tuned by the magnetic field. A comparison of different acoustic modes suggests that the slow spin fluctuations have a nematic character.

I. INTRODUCTION

The coupling of electronic instabilities to the crystal lattice plays a significant role in shaping the phase diagram of some high-T_c cuprate superconductors. The case of La-based cuprates is emblematic. Upon cooling, $La_{2-x}Ba_xCuO_4$ (LBCO) and rare-earth doped (Nd, Eu)$_y$-$La_{2-x-y}Sr_xCuO_4$ ((Nd,Eu)-LSCO) evolve from a high-T tetragonal (HTT) to a mid-T orthorhombic (OMT) and finally to a low-T tetragonal (LTT) crystal structure. The LTT order pins stripe order, a combination of mutually commensurate spin and charge modulations, initially found in Nd-LSCO [1]. Within this context sound velocity and attenuation are particularly relevant quantities. Ultrasound measurements directly probe the lattice properties and they are sensitive to any strain dependent instability.

Among the La-based cuprate family $La_{2-x}Sr_xCuO_4$ (LSCO) appears peculiar. First, the OMT-LTT structural phase transition does not occur, although LTT-like distortions exist locally [2–4]. Moreover, scattering evidence for charge ordering inside the pseudogap phase has remained elusive until recently [5–8]. In $La_{1.88}Sr_{0.12}CuO_4$ quasi-static charge modulation appears below $T_{CDW} = 70 \pm 15$ K with a maximal in-plane correlation length $\xi_{\parallel}(T_c) \simeq 30$ Å, a value practically one order of magnitude smaller than in LBCO at the same doping.

In the same compound incommensurate antiferromagnetic (AFM) correlations are also found at low field for $0.02 \leq p \lesssim 0.135$ [9]. The temperature at which these correlations appear static depends upon the probe frequency [9, 10], revealing the glassy nature of the magnetic state. However, as in other La-based compounds close to $p \approx 0.12$, one observes that the incommensurabilities of charge and spin density waves (respectively CDW and SDW) follow $2\delta_{spin} = \delta_{charge}$, a relation reminiscent of charge-spin stripe ordering [6].

Close to the hole doping level $p \approx 0.12$ elastic anomalies have been reported in both sound velocity and attenuation. Specifically, in single crystal studies and near the superconducting T_c, a broad sound velocity minimum has been observed in different acoustic modes [11, 12]. In a similar range of temperature, an attenuation maximum of longitudinal waves has been found in polycrystals [13, 14]. Different interpretations have been proposed to explain this peculiar behaviour [11–13, 15–17]. Recently, using NMR and sound velocity measurements in high magnetic field in LSCO for $p \geq 0.145$, we have shown that the anomalous sound velocity appears to be caused by a coupling of the AFM glass to the lattice [18].

In this study, we strengthen this interpretation with high magnetic field measurements of sound velocity and attenuation in LSCO $p = 0.12$. Comparing ultrasound attenuation with NMR measurements on crystals from the same batch, we reinforce the link between the slowing down of magnetic fluctuations and the ultrasound anomalies observed in the $(c_{11} - c_{12})/2$ and c_{11} elastic constants. Moreover, we show that the ultrasound prop-

*mehdi.frachet@kit.edu. Present adress : IQMT, Karlsruhe Institute für Technologie, 76021 Karlsruhe, Germany
†david.leboeuf@lncmi.cnrs.fr

erties of the $(c_{11}-c_{12})/2$ mode can be semi-quantitatively reproduced by a phenomenological dynamical susceptibility model initially developed for canonical spin glasses. Finally, by comparing different acoustic modes, we find that the spin freezing produces an enhanced susceptibility in the B_{1g} channel, which is associated with nematicity in cuprates.

This paper is organized as follows. In section II, we describe the sample studied and the experimental technique. Then, in section III we report the experimental sound velocity and attenuation measurements. We present a phenomenological model of ultrasound in spin glasses and use it to analyze the ultrasound data in section IV. Then, in section V, we discuss the magnetic field effect on the ultrasound properties, the differences between the acoustic modes studied and the symmetry of the AFM fluctuations inferred from our measurements. We summarize our conclusions in section VI.

II. METHODS

A high quality LSCO single crystal was grown by the traveling solvent floating zone method. From this crystal, three samples were cut along different crystallographic directions in order to probe different elastic constants. Typical samples dimensions are $2 \times 2 \times 2$ mm^3. The hole doping $p = 0.122 \pm 0.002$ has been determined by measuring $T_{\rm st} = 252$ K, the temperature of the HTT-OMT structural phase transition by sound velocity, as described in Ref. [18]. The different samples share a similar $T_{\rm st}$ and thus a similar doping. The superconducting transition temperature $T_{\rm c} = 29 \pm 3$ K has been determined by sound velocity, in-plane resistivity, and magnetic susceptibility measurements.

A standard pulse-echo technique with phase comparison was used to measure variations of sound velocity, $\Delta v/v$, and sound attenuation, $\Delta\alpha$ [19]. Ultrasound was generated and detected using commercial $LiNbO_3$ transducers glued onto parallel, clean and polished surfaces of the samples. The excitation frequency, ω, ranged from 50 to 300 MHz. For high symmetry propagation direction, the sound velocity variation of a given acoustic mode can be converted to the associated elastic constant change using $\Delta c_{\rm ii}/c_{\rm ii} = 2\Delta v/v$.

Zero-field and static-field experiments were performed at the LNCMI Grenoble using 20 T superconducting and 28 T resistive magnets. Field cooled conditions were used. Pulsed-fields experiments up to 60 T were carried out at the LNCMI Toulouse. In all cases, the field was applied along the crystallographic c-axis.

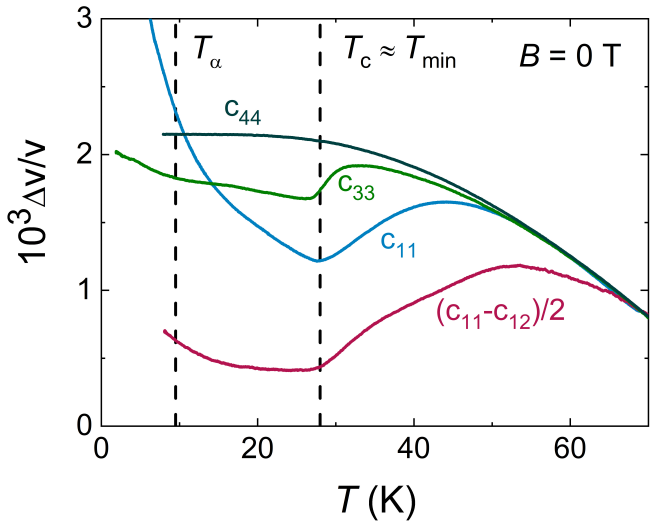

Figure 1: Sound velocity variation, $\Delta v/v$, as a function of temperature for different acoustic modes as indicated. No magnetic field is applied, the curves are arbitrarily superimposed at T=70 K. $T_{\rm min}$ refers to the minimum in the c_{11} elastic constant that coincides with the superconducting $T_{\rm c}$ in zero magnetic field. T_α indicates the spin freezing temperature at the μeV ultrasound energy scale, defined by an attenuation peak (see Fig. 2).

c_{ij}	$\vec{k}$	$\vec{u}$	ϵ_{ij}	symmetry
c_{11}	[100]	[100]	ϵ_{xx}	$A_{1g} + B_{1g}$
c_{33}	[001]	[001]	ϵ_{zz}	A_{1g}
c_{44}	[100]	[001]	ϵ_{yz}, ϵ_{zx}	E_g
$(c_{11} - c_{12})/2$	[110]	[1$\bar{1}$0]	$\epsilon_{xx} - \epsilon_{yy}$	B_{1g}

Table I: Properties of the different elastic constants measured: direction of propagation ($\vec{k}$) and polarisation ($\vec{u}$) of the acoustic wave, strain (ϵ_{ij}) and associated symmetry. The indices of elastic constants are expressed in the Voigt notation. Crystallographic directions are those of the HTT phase (D_{4h} point group).

III. RESULTS

A. Sound velocity in zero magnetic field

We begin with a zero magnetic field study of different elastic constants in LSCO $p = 0.12$ as shown in Fig. 1. The description of the different modes studied is reported in table I. The c_{44} acoustic mode follows the classical variation expected in solids: upon cooling the sound velocity increases continuously and eventually saturates at low temperature [20]. This behaviour contrasts with the c_{33} elastic constant which shows a downward jump at $T_{\rm c}$. This mean-field anomaly at the superconducting transition is expected for a longitudinal mode and is related to the specific heat jump through the Ehrenfest

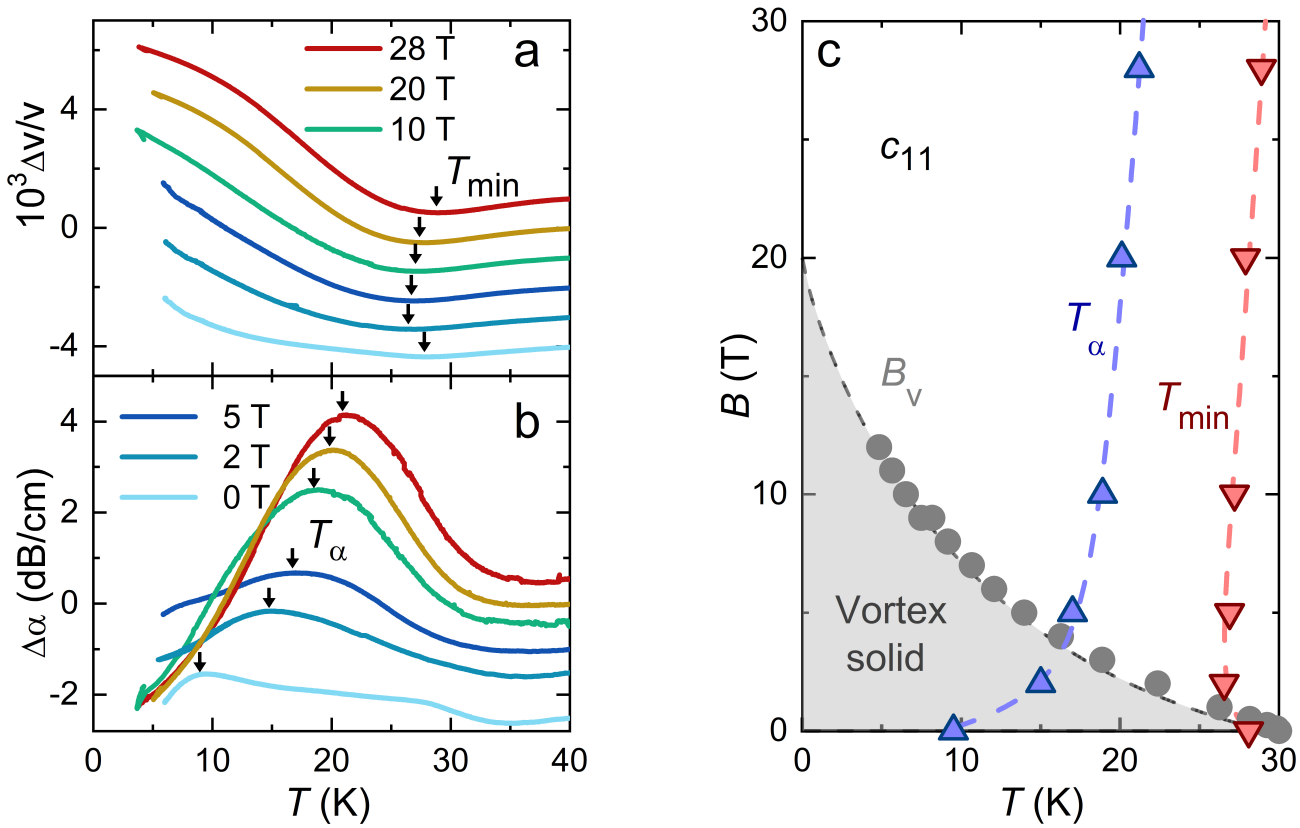

Figure 2: Static field ultrasound measurements in the c_{11} acoustic mode up to 28 T. (a) $\Delta v/v$ and (b) $\Delta\alpha$ as a function of temperature for different magnetic fields. The curves are shifted for clarity. The arrows denote $T_{\rm min}$ and T_α as indicated. (c) $B-T$ phase diagram: gray circles denote the vortex melting transition field $B_{\rm v}$ inferred from in-plane resistivity measurements, T_α (upward-pointing blue triangles) and $T_{\rm min}$ (downward-pointing red triangles) refer to the maximum in attenuation and minimum in velocity respectively. Error bars are smaller than the symbol size. Dashed lines are guides to the eye.

relationship:

$$\Delta c_{ii}(T_{\rm c}) = -\frac{\Delta C_p(T_{\rm c})}{V_{\rm mol}T_{\rm c}}\left(\frac{dT_{\rm c}}{d\epsilon_i}\right)^2 \qquad (1)$$

with $\Delta C_p(T_{\rm c})$ the specific heat jump at $T_{\rm c}$ and $V_{\rm mol}$ the molar volume. The amplitude of the anomaly, $\Delta v/v(T_{\rm c}) \simeq 0.2\times10^{-3}$, is consistent with literature values on samples with similar doping levels [21, 22].

For $T \geq T_{\rm c}$, the temperature dependence of c_{11} and $(c_{11}-c_{12})/2$ elastic constants is anomalous. In both of these modes, the normal state sound velocity decreases upon cooling, until the temperature hits $T_{\rm c}$ where it shows an upturn. Consequently, the sound velocity in these modes has a minimum at $T_{\rm min} \simeq T_{\rm c}$. Fig. 1 shows that the anomalous lattice softening appears only in acoustic modes having a $B_{1\rm g}$ strain component, namely c_{11} and $(c_{11}-c_{12})/2$. Note that so far we have not been able to measure the $B_{2\rm g}$ mode (c_{66}) for $T < T_{\rm st}$.

Finally, for $T \lesssim 15$ K or so, a rapid stiffening is observed in c_{11} upon cooling. Indeed, the sound velocity in the $T=0$ limit exceeds largely what would be expected from an extrapolation of the high temperature bare elastic constant (*e.g.* following the c_{44} elastic constant). A similar upturn is found in c_{33} and $(c_{11}-c_{12})/2$ upon cooling for $T \lesssim 15$ K, although much weaker than in c_{11}.

B. Sound velocity and attenuation in applied magnetic field

In Fig. 2 and Fig. 3 we investigate how the anomalous sound velocity, and the corresponding sound attenuation, evolve as a function of temperature at different magnetic fields, in the c_{11} and $(c_{11}-c_{12})/2$ modes respectively. In both these modes no signature of the vortex lattice is observed, as discussed in Appendix A.

The anomalous features of the zero field sound velocity in the c_{11} and $(c_{11}-c_{12})/2$ acoustic modes are enhanced by a magnetic field: both the amplitudes of the lattice softening (for $T \geq T_{\rm min}$) and stiffening ($T \leq T_{\rm min}$) increase with increasing magnetic field. For both acoustic modes an attenuation peak is found at $T_\alpha \leq T_{\rm min}$. The amplitude of this attenuation peak and T_α increase monotonically with increasing field.

The magnetic field dependencies of T_α and $T_{\rm min}$ from c_{11} measurements are shown in the phase diagram of Fig. 2(c). Within error bars, $(c_{11}-c_{12})/2$ and c_{11} show at a

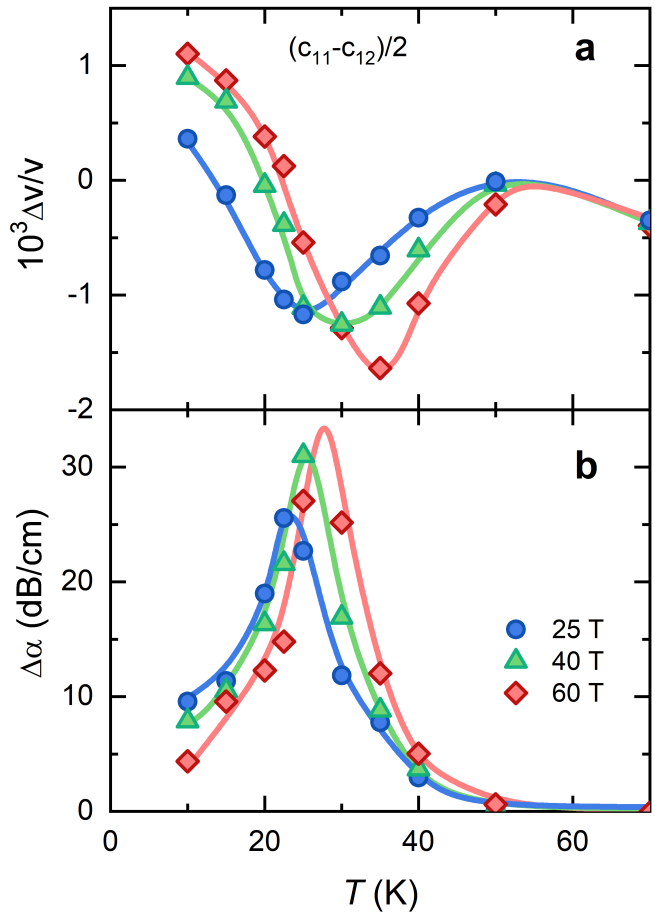

Figure 3: Temperature dependence of the $(c_{11}-c_{12})/2$ acoustic mode in pulsed-fields up to 60 T. (a) $\Delta v/v$ and (b) $\Delta\alpha$ both extracted from fixed magnetic field cuts of the pulsed-fields isotherms to which we add the zero field curve. All lines are guides to the eye.

given magnetic field similar T_α and $T_{\rm min}$. In contrast with T_α, $T_{\rm min}$ has a non-monotonic field dependence: it decreases for $0 \leq B \leq 2$ T and increases for higher fields. The initial decrease is caused by the lattice coupling to the superconducting order parameter as further detailed in Appendix B. However, for $B \geq 5$ T or so, the two temperature scales have similar field dependence, indicating that they are coupled and caused by the same phenomenon.

C. Comparison with NMR $1/T_1$

In Fig. 4 we compare the ultrasound attenuation, $\Delta\alpha$, with the ^{139}La NMR spin-lattice relaxation rate, $1/T_1$, both measured in LSCO $p = 0.12$ samples from the same batch and in a magnetic field $B = 28$ T. The comparison is striking, both quantities display remarkably similar temperature dependencies and show a maximum at comparable temperatures.

The peak in $1/T_1$ is a classical signature of spin freezing

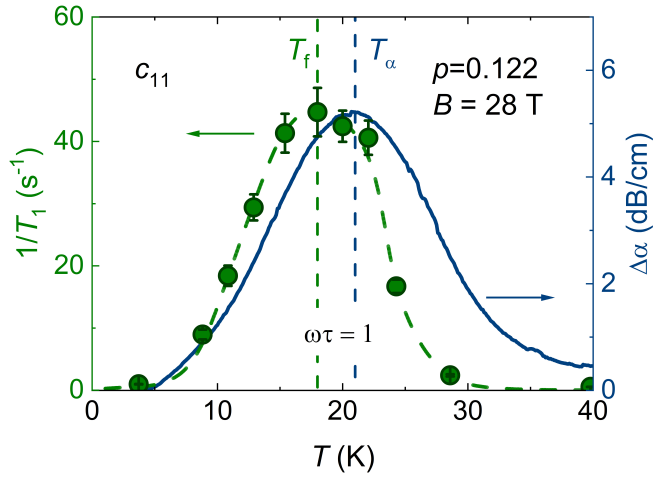

Figure 4: Comparison between the ultrasound attenuation $\Delta\alpha$ (blue line, right scale) and the ^{139}La NMR spin-lattice relaxation rate $1/T_1$ (green circle, left scale), at $B = 28$ T. NMR and ultrasound samples are from the same batch. Both physical quantities show a peak when the excitation frequency becomes equal to the frequency of the spin fluctuations, *i.e.* $\omega\tau = 1$. A phenomenological linear background has been substracted from the experimental $\Delta\alpha$ for clarity. The dashed green line is a guide to the eye.

in superconducting LSCO [23–26]. This peak is understood within the so-called Bloembergen-Purcell-Pound (BPP) model [23, 26, 27] originating from a diverging correlation time $\tau(T)$. Upon cooling, spin fluctuations are gradually slowing down. At the temperature where the condition $\omega_{\rm NMR}\tau = 1$ is fulfilled ($\omega_{\rm NMR}$ being the NMR frequency), $1/T_1$ is maximum. This temperature defines the freezing temperature $T_{\rm f}$ at the NMR timescale.

Correspondingly, Fig. 4 reveals that the ultrasound attenuation $\Delta\alpha$ is governed by a similar correlation time. At the temperature where the condition $\omega_{\rm US}\tau = 1$ is met, with $\omega_{\rm US}$ the ultrasound frequency, a peak in the ultrasound attenuation is observed. The good agreement between $T_{\rm f}$ and T_α is provided by the fact that $\omega_{\rm NMR} \approx \omega_{\rm US} \approx 10^8$ Hz. Finally, note that the small difference observed between $\Delta\alpha$ and $1/T_1$ could arise from a small variation in doping level between the two samples, but also from a disparity in the way these probes couple to the magnetic moments. This is discussed in the next section.

IV. MODELLING

A broad sound velocity minimum at $T_{\rm min}$ [28–30] and an attenuation peak at $T_\alpha \leq T_{\rm min}$ [28, 31] are common characteristics of - insulating or metallic - canonical spin glasses around the spin freezing temperature. The sound velocity and attenuation of a cobalt fluorophosphorate spin glass shown in Fig. 5(a) exemplify those

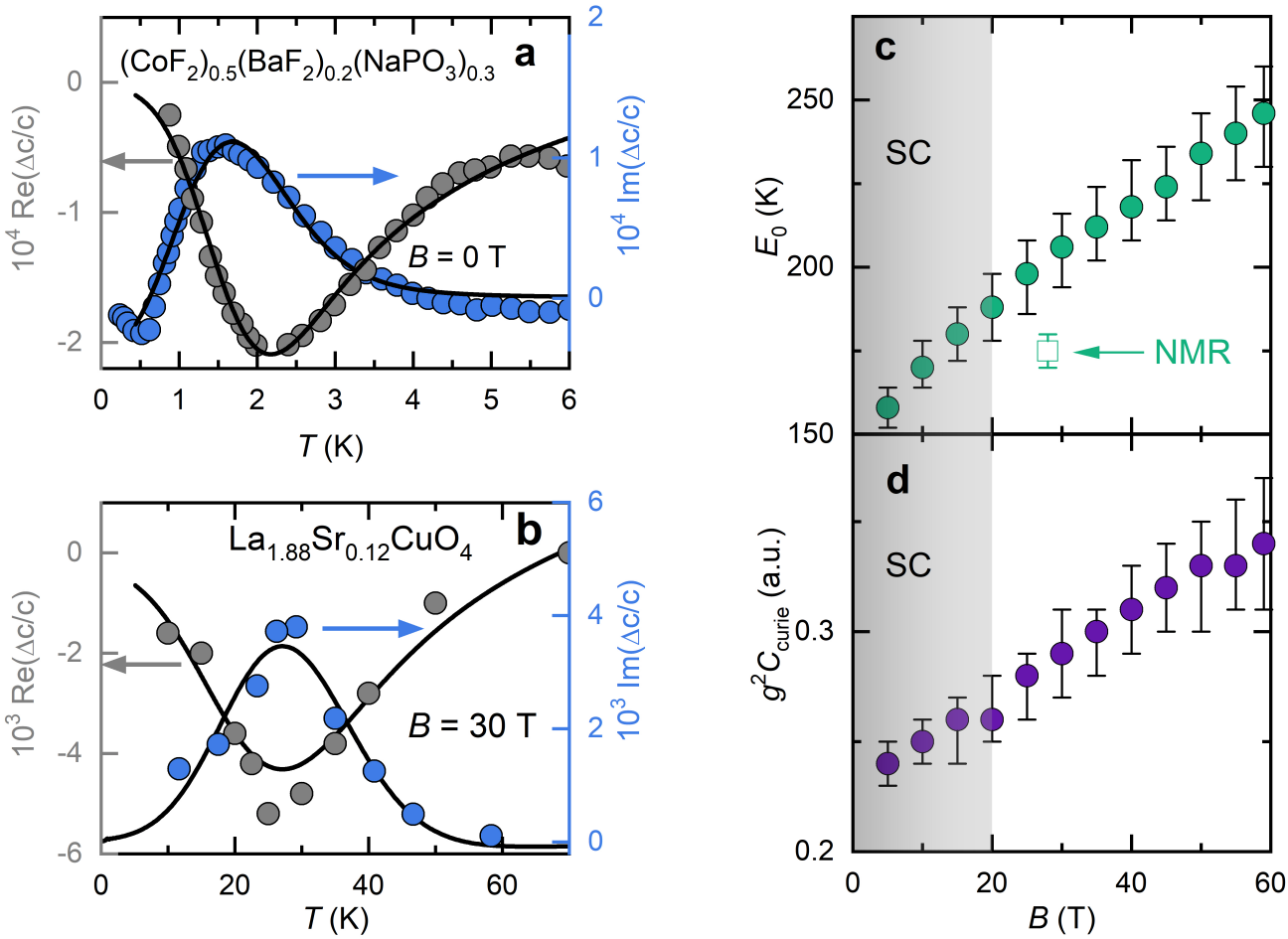

Figure 5: Fitting of the experimental $\Re\mathsf{e}\,(\Delta c/c)$ (gray circles, left scale) and $\Im\mathsf{m}\,(\Delta c/c)$ (blue circles, right scale) for (a) the cobalt fluorophosphorate canonical spin glass in a longitudinal acoustic mode reproduced from Ref.[28] and (b) LSCO $p = 0.12$ at $B = 30$ T in the $(c_{11} - c_{12})/2$ transverse mode. In panels (a) and (b) a background sound velocity has been subtracted. The black lines are fit to the data using the dynamical susceptibility model. Fitting parameters for cobalt fluorophosphate are $E_0 \approx 18$ K and $g^2 C_{\rm curie} \approx 10^{-3}$ a.u.. Fitting parameters for LSCO $p = 0.12$ are shown in panels (c) E_0 and (d) $g^2 C_{\rm curie}$. The other two free parameters, $g^2\chi_0 \approx -4.5$ a.u. and $\Delta E_0 \approx 70$ K, don't show any significant field dependence. For comparison E_0 extracted from NMR $1/T_1$ at 28 T found in Fig. 4 (empty square) is also shown. The error bars on a single parameter are estimated by monitoring the error of the fit with all other parameters fixed.

features. The comparison with the elastic properties of LSCO $p = 0.12$ in the $(c_{11} - c_{12})/2$ mode shown in Fig. 5(b) is striking: both systems show remarkably similar phenomenology.

In the following, we focus on the transverse $(c_{11}-c_{12})/2$ acoustic mode shown in Fig. 3 and demonstrate that it can be semi-quantitatively reproduced by a phenomenological model developed for spin glasses. The strong increase observed in $c_{11}(T)$ at low temperature is not explained by this model and will be discussed later.

We use the phenomenological dynamical susceptibility model developed by Doussineau *et al.* [28, 32]. Sound velocity and attenuation are expressed in terms of a complex elastic constant, $c(\omega, T)$:

$$c(\omega, T) = c_0 \left[1 - g^2 \chi_4(\omega, T)\right] \tag{2}$$

With c_0 the bare elastic constant, g the spin-phonon coupling constant and ω the ultrasound measurement frequency. Ultrasound quantities are deduced through:

$$\Delta v/v = \frac{1}{2}\Re\mathsf{e}\,(\Delta c/c) \tag{3}$$

$$\Delta\alpha(\mathsf{dB/cm}) = \frac{\omega}{v}\frac{10}{\log(10)}\Im\mathsf{m}\,(\Delta c/c) \tag{4}$$

Here $\chi_4(\omega, T)$ is a dynamical susceptibility defined as:

$$\chi_4(\omega, T) = \int \frac{d\tau_4}{\tau_4}\frac{\chi_4(\omega = 0, T)}{1 + i\omega\tau_4} \tag{5}$$

$\chi_4(\omega = 0, T)$ is a static susceptibility and $\tau_4(T)$ is the correlation time of the spin fluctuations. In our

case, since $S = 1/2$, the magneto-acoustic coupling arises from the Waller mechanism (also called exchange-striction mechanism), *i.e.* a modulation of the exchange interaction by the strain [19]. Consequently, the associated susceptibility is quadrupolar and the correlation time is involved in a four-spin correlation function. In contrast, the $1/T_1$ NMR relaxation rate is governed by a correlation time $\tau_2(T)$ which is involved in a two-spin correlation function. This can produce slight differences between $\Delta\alpha$ and $1/T_1$ in Fig. 4 [33]. We use the following expressions for $\tau_4(T)$ and $\chi_4(\omega = 0, T)$:

$$\tau_4(T) = \tau_\infty \exp(E_0/T) \tag{6}$$

$$\chi_4(\omega = 0, T) = \chi_0 + \frac{C_{\text{curie}}}{T} \tag{7}$$

C_{curie} controls the amplitude of the lattice softening for $T \geq T_{\text{min}}$, E_0 is an energy scale that governs T_{min} and T_α, χ_0 is the constant term of the susceptibility and finally τ_∞ is the correlation time of spin fluctuations for $T \gg E_0$. Note that Eq. 6 and Eq. 7 are motivated by an analysis of ^{139}La NMR $1/T_1$ [23, 26] and ac-susceptibility measurements in the AFM glass of LSCO [34, 35] respectively. As inferred from various experiments [36], the value of τ_∞ is fixed to $\exp(-30) \simeq 10^{-13}$ s. Moreover, as usually done in spin glasses [28, 37], and especially in the AFM glass phase of LSCO [26, 36], we consider that $\tau_4(T)$ is inhomogeneous using a gaussian-distribution of E_0 with full width at half maximum $2\Delta E_0$. Within this framework it is possible to fit simultaneously $\Delta v/v$ and $\Delta\alpha$, and to extract both E_0 and $g^2 C_{\text{curie}}$ as a function of magnetic field. A representative example is shown on Fig. 5(b): the model reproduces most of the salient features seen in the two ultrasound quantities.

The evolution of the fitting parameters is shown in Fig. 5(c, d). Up to $B = 60$ T - *i.e.* well above our $T \to 0$ extrapolation of the vortex melting field B_{v} on Fig. 2(c) - E_0 and $g^2 C_{\text{curie}}$ increase continuously. The former increase is related to the non saturating values of the temperature scales T_α and T_{min}. The latter is explained by the continuous increase of the amplitudes of the lattice softening and attenuation peak up to 60 T (see Fig. 3).

The NMR $1/T_1$ data at $B = 28$ T shown in Fig. 4 can be fitted with the BPP formula using Eq. 6 for $\tau_2(T)$ and a gaussian distribution of activation energy E_0 [26, 38]. This parametrization of $1/T_1$ data yields an activation energy in fair agreement with E_0 inferred from ultrasound data (see Fig. 5(c)). It has been suggested previously that the activation energy is analogous to the spin-stiffness $2\pi\rho_s$ [24, 38, 39]. The value of $E_0 \approx 200$ K found here for $B = 20$ T is comparable to what is obtained in Nd-LSCO $x = 0.12$ in zero magnetic field [24, 39, 40]. It is an order of magnitude smaller than the spin stiffness of the antiferromagnetic parent compound La_2CuO_4 where $2\pi\rho_s \approx J$ [41].

Finally, in the paramagnetic state of a classical Néel AFM $C_{\text{curie}} \propto \mu^2$, where μ is the magnetic moment. Since the dynamical susceptibility model is purely phenomenological, we cannot extract microscopic information. As such, the increase of $g^2 C_{\text{curie}}$ with magnetic field (see Fig. 5(d)) could originate from an enhanced μ [42, 43] or from an increased magnetic volume [44].

V. DISCUSSION

Let us summarize our results so far. **(i)** The $(c_{11} - c_{12})/2$ and c_{11} modes show a softening for $T \geq T_{\text{min}}$ and a hardening for $T \leq T_{\text{min}}$. Those features are enhanced by magnetic field and survive when superconductivity is strongly suppressed by the field. Consequently, neither feature is caused by superconductivity. We attribute this broad sound velocity minimum to the freezing of the AFM glass. **(ii)** The striking similarity of the ultrasound attenuation with the NMR relaxation rate $1/T_1$ shows that the AFM glass is also causing the anomalous attenuation peak in high magnetic field. **(iii)** The behaviour of the $(c_{11} - c_{12})/2$ elastic constant found in LSCO $p = 0.12$ in high magnetic field is remarkably similar to what is found in canonical spin glasses. A dynamical susceptibility model, developed in the context of spin glasses, reproduces all features of the anomalous ultrasound properties in the $(c_{11} - c_{12})/2$ mode.

The similar decrease of T_{min} and T_{c} with magnetic field $B \leq 14$ T in LSCO at $p \approx 0.14$ has previously motivated a scenario in which a competing lattice instability - that produces a lattice softening for $T > T_{\text{c}}$ - is quenched by the onset of superconductivity that induces a hardening for $T < T_{\text{c}}$ [12]. While we observe the same behaviour in LSCO $p = 0.12$ for $B \leq 2$T (see Appendix B for more details), this scenario does not hold at higher field where we observe an increase of T_{min}. All measurements reported here in LSCO $p = 0.12$ support the interpretation that the ultrasound anomalies are caused by the AFM glass phase via spin-phonon coupling [18].

In the following we discuss some implications of the aforementioned results. In particular we comment on the magnetic field effect on the ultrasound properties, the relation of this study with previous elastic experiments and the symmetry of the AFM quasi-static fluctuations.

A. The special coupling with $B_{1\text{g}}$ strain

In canonical spin glasses such as cobalt fluorophosphorate, the magnetic moments are frozen in a random manner (note however that metallic spin glass CuMn show short ranged (~ 20 Å) SDW correlations [45]). Consequently, longitudinal and transverse acoustic modes couple similarly to the spins in such systems (see Ref. [32]). The magnetic moments of LSCO have similar dynamical properties as canonical spin glasses: they gradually freeze as the system is cooled down, such that the onset temper-

ature depends on the probe frequency [9, 10]. However, the moments in LSCO arrange in a pattern displaying incommensurate AFM character, and Bragg peaks indicating correlation lengths as high as ~ 200 Å in LSCO $x = 0.12$ are observed in neutron diffraction experiments [42, 46–48]. Consequently in LSCO the coupling between the frozen spins and the lattice varies dramatically from one mode to another, as shown in Fig. 1. The anomalous softening for $T \geq T_{\rm min}$ is observed only in modes transforming according to the $B_{1\rm g}$ irreducible representation (see Table I and Fig. 1). Note however, that we cannot exclude a similar coupling of the AFM glass to $B_{2\rm g}$ mode. Nonetheless this suggests a special role of the $B_{1\rm g}$ mode.

Within the framework of the dynamical susceptibility model, the lattice softening in the B_{1g} mode is caused by the growth of a Curie-like susceptibility $\chi_4(\omega = 0, T)$. Eq. 2 is reminiscent of the elastic constant $c = {\rm d}^2F/{\rm d}\epsilon^2$ calculated using a Landau free energy F containing a bilinear coupling $F_{\rm c} = g\epsilon Q$ [19], with ϵ a strain and Q an order parameter. Indeed, within such a model, the softening is directly related to the increasing mean-field susceptibility of Q, $\Delta v/v \propto -g^2\chi_Q$. For this bilinear coupling to exist, both ϵ and Q must transform according to the same irreducible representation. In this context, our result would suggest that the order parameter (and the fluctuations) associated with the AFM glass has a B_{1g}, *i.e.* nematic, character.

Although conjectural in the absence of a measurement of the $B_{2\rm g}$ mode, this interpretation of the ultrasound data is evocative of the B_{1g} susceptibility observed by symmetry-resolved Raman scattering in LSCO at $x = 0.10$ [49]. It is consistent with evidence of charge and spin stripe orders in this compound [6, 48, 50, 51]. Nematicity can indeed result from fluctuating stripes [52]. We note that, at this doping, the observed B_{1g} susceptibility develops well below the pseudogap temperature $T^\star$. Indeed, our ultrasound experiment does not detect any significant B_{1g} susceptibility in the vicinity of $T^\star \approx 130$ K [53]. The lack of B_{1g} susceptibility at the pseudogap temperature is also reported in symmetry-resolved electronic Raman scattering experiments in $Bi_2Sr_2CaCu_2O_{8+\delta}$ [54]. The onset temperature of our detection of B_{1g} susceptibility is actually comparable to the CDW onset temperature $T_{\rm CDW} = 70 \pm 15$ K [5–7]. This suggests that, in LSCO $p = 0.12$, charge-stripe order triggers slow magnetic fluctuations [55–57] with nematic character.

B. The effect of the magnetic field

Previous neutron scattering and μSR experiments have shown that the magnetism of LSCO at $p \approx 0.12$ is enhanced by a magnetic field [42, 43, 58–61], and this effect has been ascribed to a competition between superconducting and AFM order parameters. In line with this interpretation, we observe that the ultrasound signatures of the AFM glass are strengthened by a magnetic field (see Fig. 2, 3 and 5). The magnetic field dependence

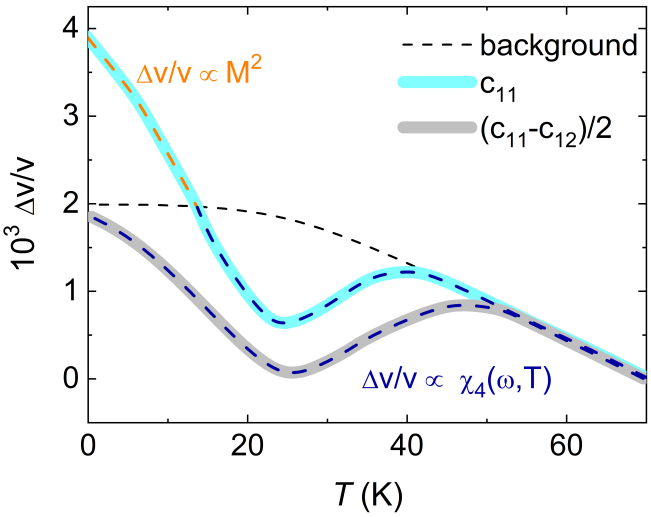

Figure 6: Schematic representation of the sound velocity of the $(c_{11} - c_{12})/2$ (grey) and c_{11} (cyan) modes in LSCO $p = 0.12$. Black dashed line is the background elastic constant arising from anharmonicity of ionic potential [20]. $(c_{11} - c_{12})/2$ can be fully reproduced by the dynamical susceptibility model involving $\chi_4(\omega, T)$ (dashed blue line). For $T \to 0$, the difference between the sound velocity of the $(c_{11} - c_{12})/2$ mode and its background tends to zero. This contrasts with the behaviour of c_{11}. For $T \to 0$, the sound velocity of the c_{11} mode is larger than the background sound velocity. This means that in addition to the contribution from $\chi_4(\omega, T)$ (dashed blue line) that causes the minimum in c_{11}, another component contributes at low T. As discussed in the text, a contribution proportional to M^2 (dashed orange line) could explain the rapid increase of c_{11} at low temperature.

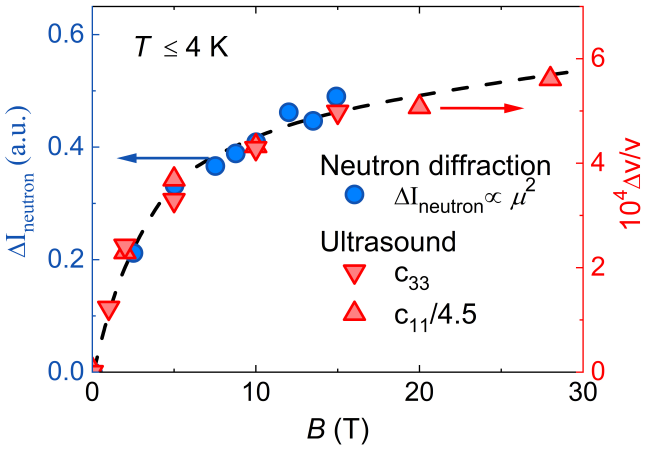

Figure 7: Comparison between the magnetic field dependence of the superlattice Bragg peak intensity of incommensurate AFM seen by neutron diffraction, $\Delta I_{\rm neutron}$ (blue circles, left scale), and the sound velocity, $\Delta v/v$, in the c_{11} and c_{33} acoustic modes (up and down red triangles respectively, right scale). The neutron diffraction intensity is reproduced from Ref. [42]. The sound velocity in the c_{11} mode is divided by a factor 4.5. The sound velocity measurements presented here are taken at $T \leq 4$ K in field-cooled conditions. The dashed line is a guide to the eye.

of the ultrasound properties does not saturate up to 60 T and the magnetic field induced softening appears at temperatures as high as $T \approx 50$ K (see Fig. 3). These observations are puzzling since at this doping $T_c \approx 29$ K and the extrapolation of the vortex melting line leads to $B_v(T \longrightarrow 0) \approx 20$ T. This raises important questions on the effect of magnetic fields on the magnetic freezing and the possible resilience of superconducting fluctuations in high field.

We note that this behaviour is reminiscent of the magnetoresistance producing an upturn in the resistivity of superconducting LSCO in high fields. This magnetoresistance is observed up to $T \simeq 100$ K at the doping level $p = 0.12$ [62]. The spin freezing has been previously discussed as a cause of the resistivity upturn in La-based cuprates [63–67]. Consequently, it is possible that the large magnetoresistance observed in LSCO $p = 0.12$ above T_c is related to the field-induced gradual slowing down of magnetic fluctuations observed here.

C. Differences between c_{11} and $(c_{11} - c_{12})/2$

Finally, we discuss the differences between the c_{11} and $(c_{11} - c_{12})/2$ modes. As discussed above, the strength of the magneto-acoustic coupling is largest in the $(c_{11} - c_{12})/2$ mode, where the largest softening is observed (see Fig. 1). The second difference between the response in these two modes is the field-enhanced hardening that is seen in c_{11} at low temperature. The situation is schematically depicted in Fig. 6. In the $(c_{11} - c_{12})/2$ mode, the difference between the measured sound velocity in the $T \to 0$ limit and the background velocity is negligibly small. On the other hand this difference is significant in the c_{11} mode, with the measured sound velocity being larger than the background velocity. This behaviour echoes the results from previous studies performed on polycrystals. Earlier ultrasound studies suggested that this behaviour can be caused by LTT distortions [13, 68]. On the other hand, anelastic experiments implied a coupling between strain and AFM glass domain wall motion [69].Those studies are discussed in greater details in Appendix C.

Here we propose an alternative mechanism that could cause the low temperature stiffening in the c_{11} mode. We start by noticing that a stiffening is also observed in the c_{33} mode for $T \lesssim T_\alpha$ (see Fig. 1). As shown in Fig. 7, the low temperature increase of the sound velocity in both the c_{11} and c_{33} modes has a field dependence that scales with the increase in μ^2, the ordered moment squared inferred from neutron diffraction experiment, as discussed previously [13, 17]. This scaling can be explained by invoking a biquadratic coupling $F_c = \lambda\epsilon^2 M^2$ with M the magnetization, and λ a coupling constant. Note that F_c is symmetry-allowed for all elastic constants of Table I. This coupling produces $\Delta v/v \propto \lambda M^2$ and can naturally account for the experimental observations if we assume that the coupling constant λ is larger for longitudinal modes (c_{11} and c_{33}) than it is for transverse modes (c_{44} and $(c_{11} - c_{12})/2$).

VI. SUMMARY

In summary, we studied sound velocity and attenuation in $La_{1.88}Sr_{0.12}CuO_4$ in high magnetic field. The behaviour of the c_{11} and $(c_{11} - c_{12})/2$ elastic constants is highly anomalous. By comparing the anomalies with ^{139}La NMR $1/T_1$ we confirm that they originate from the AFM glass phase via a magneto-acoustic coupling. A semi-quantitative analysis of this contribution is made based on a phenomenological model of spin glass systems. Our ultrasound data points toward a strong competition between spin freezing and superconductivity in high magnetic field. A symmetry analysis reveals that the slowing down of spin fluctuations could be associated with a growing nematic susceptibility.

ACKNOWLEDGMENTS

We thank A. Böhmer, I. Paul and D. Campbell for fruitful discussions, as well as D. Destraz and O. Ivashko for their assistance with sample preparation. Part of this work was performed at the LNCMI, a member of the European Magnetic Field Laboratory (EMFL). Work at the LNCMI was supported by the Laboratoire d'Excellence LANEF (ANR-10-LABX-51-01), French Agence Nationale de la Recherche (ANR) grant ANR-19-CE30-0019-01 (Neptun) and EUR grant NanoX n°ANR-17-EURE-0009. Work in Zürich was supported by the Swiss National Science Foundation.

[1] J. M. Tranquada, B. J. Sternlieb, J. D. Axe, Y. Nakamura, and S. Uchida. Evidence for stripe correlations of spins and holes in copper oxide superconductors. *Nature*, 375:561–563, 1995.

[2] E. S. Božin, S. J. L. Billinge, G. H. Kwei, and H. Takagi. Charge-stripe ordering from local octahedral tilts: Underdoped and superconducting $La_{2-x}Sr_xCuO_4(0 < x < 0.30)$. *Phys. Rev. B*, 59:4445–4454, Feb 1999.

[3] A. Bianconi, N. L. Saini, A. Lanzara, M. Missori, T. Rossetti, H. Oyanagi, H. Yamaguchi, K. Oka, and T. Ito. Determination of the local lattice distortions in the CuO_2 plane of $La_{1.85}Sr_{0.15}CuO_4$. *Phys. Rev. Lett.*, 76:3412–3415, 1996.

[4] N. L. Saini, A. Lanzara, H. Oyanagi, H. Yamaguchi, K. Oka, T. Ito, and A. Bianconi. Local lattice instability and stripes in the CuO_2 plane of the $La_{1.85}Sr_{0.15}CuO_4$

system by polarized XANES and EXAFS. *Phys. Rev. B*, 55:12759–12769, 1997.

[5] V. Thampy, M. P. M. Dean, N. B. Christensen, L. Steinke, Z. Islam, M. Oda, M. Ido, N. Momono, S. B. Wilkins, and J. P. Hill. Rotated stripe order and its competition with superconductivity in $La_{1.88}Sr_{0.12}CuO_4$. *Phys. Rev. B*, 90:100510, 2014.

[6] T. P. Croft, C. Lester, M. S. Senn, A. Bombardi, and S. M. Hayden. Charge density wave fluctuations in $La_{2-x}Sr_xCuO_4$ and their competition with superconductivity. *Phys. Rev. B*, 89:224513, 2014.

[7] N. B. Christensen et al. Bulk charge stripe order competing with superconductivity in $La_{2-x}Sr_xCuO_4$ ($x = 0.12$). *arXiv*, 1404.3192, 2014.

[8] J. J. Wen, H. Huang, S. J. Lee, H. Jang, J. Knight, Y. S. Lee, M. Fujita, K. M. Suzuki, S. Asano, S. A. Kivelson, C. C. Kao, and J. S. Lee. Observation of two types of charge-density-wave orders in superconducting $La_{2-x}Sr_xCuO_4$. *Nature Communications*, 10:3269, 2019.

[9] M.-H. Julien. Magnetic order and superconductivity in $La_{2-x}Sr_xCuO_4$: a review. *Physica B: Condensed Matter*, 329-333:693 – 696, 2003. Proceedings of the 23rd International Conference on Low Temperature Physics.

[10] A. T. Rømer, J. Chang, N. B. Christensen, B. M. Andersen, K. Lefmann, L. Mähler, J. Gavilano, R. Gilardi, Ch. Niedermayer, H. M. Rønnow, A. Schneidewind, P. Link, M. Oda, M. Ido, N. Momono, and J. Mesot. Glassy low-energy spin fluctuations and anisotropy gap in $La_{2-x}Sr_xCuO_4$. *Phys. Rev. B*, 87:144513, 2013.

[11] T. Suzuki, T. Goto, K. Chiba, T. Shinoda, T. Fukase, H. Kimura, K. Yamada, M. Ohashi, and Y. Yamaguchi. Observation of modulated magnetic long-range order in $La_{1.88}Sr_{0.12}CuO_4$. *Phys. Rev. B*, 57:R3229–R3232, 1998.

[12] M. Nohara, T. Suzuki, Y. Maeno, T. Fujita, I. Tanaka, and H. Kojima. Interplay between lattice softening and high-T_c superconductivity in $La_{1.86}Sr_{0.14}CuO_4$. *Phys. Rev. Lett.*, 70:3447–3450, 1993.

[13] J. F. Qu, Y. Q. Zhang, X. L. Lu, X. Q. Xiang, Y. L. Liao, G. Li, and X. G. Li. Ultrasonic study on magnetic-field-induced stripe order in $La_{1.88-x}Sr_{0.12}Ba_xCuO_4$. *Applied Physics Letters*, 89(16):162508, 2006.

[14] J.F. Qu, Y.Q. Zhang, X.Q. Xiang, X.L. Lu, and X.G. Li. Effect of magnetic field on the charge-stripe phase in $La_{2-x-y}Nd_ySr_xCuO_4$: An ultrasonic attenuation study. *Materials Science and Engineering: A*, 442(1):216 – 219, 2006. Proceedings of the 14th International Conference on Internal Friction and Mechanical Spectroscopy.

[15] T. Hanaguri, T. Fukase, T. Suzuki, I. Tanaka, and H. Kojima. Elastic anomalies in a $La_{1.85}Sr_{0.15}CuO_4$ single crystal under high magnetic fields. *Physica B: Condensed Matter*, 194-196:1579 – 1580, 1994.

[16] S. Sakita, T. Suzuki, F. Nakamura, M. Nohara, Y. Maeno, and T. Fujita. Elastic softening in single-crystalline $La_{2-x}Sr_xCuO_4$ around x=1/8. *Physica B: Condensed Matter*, 219-220:216 – 218, 1996. PHONONS 95.

[17] Jean-Yves Prieur and Jacques Joffrin. Ultrasonic velocity variations in $La_{2-x}Sr_xCuO_4$ single crystals. *physica status solidi (c)*, 1(11):3061–3064, 2004.

[18] M. Frachet, I. Vinograd, R. Zhou, S. Benhabib, S. Wu, H. Mayaffre, S. Krämer, S. K. Ramakrishna, A. Reyes, J. Debray, T. Kurosawa, N. Momono, M. Oda, S. Komiya, S. Ono, M. Horio, J. Chang, C. Proust, D. LeBoeuf, and M.-H. Julien. Hidden magnetism at the pseudogap critical point of a high temperature superconductor. *Nature Physics*, 16:1064, 2020.

[19] B. Luthi. Physical acoustics in the solid state. 2005.

[20] Y. P. Varshni. Temperature dependence of the elastic constants. *Phys. Rev. B*, 2:3952–3958, 1970.

[21] M. Nohara, T. Suzuki, Y. Maeno, T. Fujita, I. Tanaka, and H. Kojima. Unconventional lattice stiffening in superconducting $La_{2-x}Sr_xCuO_4$ single crystals. *Phys. Rev. B*, 52:570–580, 1995.

[22] F. Gugenberger, C. Meingast, G. Roth, K. Grube, V. Breit, T. Weber, H. Wühl, S. Uchida, and Y. Nakamura. Uniaxial pressure dependence of T_c from high-resolution dilatometry of untwinned $La_{2-x}Sr_xCuO_4$ single crystals. *Phys. Rev. B*, 49:13137–13142, May 1994.

[23] V. F. Mitrović, M.-H. Julien, C. de Vaulx, M. Horvatić, C. Berthier, T. Suzuki, and K. Yamada. Similar glassy features in the ^{139}La NMR response of pure and disordered $La_{1.88}Sr_{0.12}CuO_4$. *Phys. Rev. B*, 78:014504, 2008.

[24] A. W. Hunt, P. M. Singer, A. F. Cederström, and T. Imai. Glassy slowing of stripe modulation in $(\mathrm{La,Eu,Nd})_{2-x}(\mathrm{Sr,Ba})_x\mathrm{CuO_4}$: $\mathrm{A}^{63}\mathrm{Cu}$ and ^{139}La NQR study down to 350 mK. *Phys. Rev. B*, 64:134525, Sep 2001.

[25] B. Simovič, P. C. Hammel, M. Hücker, B. Büchner, and A. Revcolevschi. Experimental evidence for a glass forming stripe liquid in the magnetic ground state of $La_{1.65}Eu_{0.2}Sr_{0.15}CuO_4$. *Phys. Rev. B*, 68:012415, Jul 2003.

[26] N. J. Curro, P. C. Hammel, B. J. Suh, M. Hücker, B. Büchner, U. Ammerahl, and A. Revcolevschi. Inhomogeneous low frequency spin dynamics in $La_{1.65}Eu_{0.2}Sr_{0.15}CuO_4$. *Phys. Rev. Lett.*, 85:642–645, Jul 2000.

[27] N. Bloembergen, E. M. Purcell, and R. V. Pound. Relaxation effects in nuclear magnetic resonance absorption. *Phys. Rev.*, 73:679–712, 1948.

[28] P. Doussineau, A. Levelut, M. Matecki, J. P. Renard, and W. Schön. Acoustic and magnetic studies of an insulating spin glass. *Europhysics Letters (EPL)*, 3(2):251–258, 1987.

[29] T. C. Hsu and J. B. Marston. Measurement of ultrasound velocity in the spin-glass CuMn. *Journal of Applied Physics*, 61(5):2074–2077, 1987.

[30] G. F. Hawkins and R. L. Thomas. Ultrasonic studies of spin glasses: CuMn. *Journal of Applied Physics*, 49(3):1627–1629, 1978.

[31] E. Gaganidze and P. Esquinazi. Temperature dependence of the sound attenuation at the spin glass transition of metallic spin glasses. *Czechoslovak Journal of Physics*, 46:2227–2228, 1996.

[32] P. Doussineau, A. Levelut, and W. Schön. Acoustic susceptibility of an insulating spin-glass. *Zeitschrift für Physik B Condensed Matter*, 73:89–102, 1988.

[33] U. G. Volkmann, R. Böhmer, A. Loidl, K. Knorr, U. T. Höchli, and S. Haussühl. Dipolar and quadrupolar freezing in $(\mathrm{KBr})_{1-x}(\mathrm{KCN})_x$. *Phys. Rev. Lett.*, 56:1716–1719, Apr 1986.

[34] S. Wakimoto, S. Ueki, Y. Endoh, and K. Yamada. Systematic study of short-range antiferromagnetic order and the spin-glass state in lightly doped $La_{2-x}Sr_xCuO_4$. *Phys. Rev. B*, 62:3547–3553, 2000.

[35] F. C. Chou, N. R. Belk, M. A. Kastner, R. J. Birgeneau, and Amnon Aharony. Spin-glass behavior in $La_{1.96}Sr_{0.04}CuO_4$. *Phys. Rev. Lett.*, 75:2204–2207, 1995.

[36] R. S. Markiewicz, F. Cordero, A. Paolone, and R. Cantelli. Cluster spin-glass distribution functions in $La_{2-x}Sr_xCuO_4$. *Phys. Rev. B*, 64:054409, Jul 2001.

[37] L. Lundgren, P. Svedlindh, and O. Beckman. Anomalous time dependence of the susceptibility in a Cu(Mn) spin glass. *Journal of Magnetism and Magnetic Materials*, 31-34:1349 – 1350, 1983.

[38] I. Vinograd. Études par résonance magnétique nucléaire des ordres en compétitions dans les cuprates supraconducteurs. *PhD Thesis*, Université Grenoble Alpes, 2019.

[39] G. B. Teitel'baum, I. M. Abu-Shiekah, O. Bakharev, H. B. Brom, and J. Zaanen. Spin dynamics and ordering of a cuprate stripe antiferromagnet. *Phys. Rev. B*, 63:020507, Dec 2000.

[40] J. M. Tranquada, N. Ichikawa, and S. Uchida. Glassy nature of stripe ordering in $La_{1.6-x}Nd_{0.4}Sr_xCuO_4$. *Phys. Rev. B*, 59:14712–14722, Jun 1999.

[41] B. Keimer, N. Belk, R. J. Birgeneau, A. Cassanho, C. Y. Chen, M. Greven, M. A. Kastner, A. Aharony, Y. Endoh, R. W. Erwin, and G. Shirane. Magnetic excitations in pure, lightly doped, and weakly metallic La_2CuO_4. *Phys. Rev. B*, 46:14034–14053, Dec 1992.

[42] J. Chang, Ch. Niedermayer, R. Gilardi, N. B. Christensen, H. M. Rønnow, D. F. McMorrow, M. Ay, J. Stahn, O. Sobolev, A. Hiess, S. Pailhes, C. Baines, N. Momono, M. Oda, M. Ido, and J. Mesot. Tuning competing orders in $La_{2-x}Sr_xCuO_4$ cuprate superconductors by the application of an external magnetic field. *Phys. Rev. B*, 78:104525, 2008.

[43] B. Lake, H. M. Rønnow, N. B. Christensen, G. Aeppli, K. Lefmann, D. F. McMorrow, P. Vorderwisch, P. Smeididl, N. Mangkorntong, T. Sasagawa, M. Nohara, H. Takagi, and T. E. Mason. Antiferromagnetic order induced by an applied magnetic field in a high-temperature superconductor. *Nature*, 415:299–302, 2002.

[44] A. T. Savici, Y. Fudamoto, I. M. Gat, T. Ito, M. I. Larkin, Y. J. Uemura, G. M. Luke, K. M. Kojima, Y. S. Lee, M. A. Kastner, R. J. Birgeneau, and K. Yamada. Muon spin relaxation studies of incommensurate magnetism and superconductivity in stage-4 $La_2CuO_{4.11}$ and $La_{1.88}Sr_{0.12}CuO_4$. *Phys. Rev. B*, 66:014524, Jul 2002.

[45] J. A. Mydosh. *Spin Glasses: an experimental introduction*. Taylor and Francis, 1993.

[46] K. Yamada, C. H. Lee, K. Kurahashi, J. Wada, S. Wakimoto, S. Ueki, H. Kimura, Y. Endoh, S. Hosoya, G. Shirane, R. J. Birgeneau, M. Greven, M. A. Kastner, and Y. J. Kim. Doping dependence of the spatially modulated dynamical spin correlations and the superconducting-transition temperature in $La_{2-x}Sr_xCuO_4$. *Phys. Rev. B*, 57:6165–6172, 1998.

[47] M. Fujita, K. Yamada, H. Hiraka, P. M. Gehring, S. H. Lee, S. Wakimoto, and G. Shirane. Static magnetic correlations near the insulating-superconducting phase boundary in $La_{2-x}Sr_xCuO_4$. *Phys. Rev. B*, 65:064505, 2002.

[48] S. Wakimoto, R. J. Birgeneau, M. A. Kastner, Y. S. Lee, R. Erwin, P. M. Gehring, S. H. Lee, M. Fujita, K. Yamada, Y. Endoh, K. Hirota, and G. Shirane. Direct observation of a one-dimensional static spin modulation in insulating $La_{1.95}Sr_{0.05}CuO_4$. *Phys. Rev. B*, 61:3699–3706, 2000.

[49] L. Tassini, F. Venturini, Q.-M. Zhang, R. Hackl, N. Kikugawa, and T. Fujita. Dynamical properties of charged stripes in $La_{2-x}Sr_xCuO_4$. *Phys. Rev. Lett.*, 95:117002, Sep 2005.

[50] Yoichi Ando, Kouji Segawa, Seiki Komiya, and A. N. Lavrov. Electrical resistivity anisotropy from self-organized one dimensionality in high-temperature superconductors. *Phys. Rev. Lett.*, 88:137005, Mar 2002.

[51] J. Choi, Q. Wang, S. Jöhr, N. B. Christensen, J. Küspert, D. Bucher, D. Biscette, M. Hücker, T. Kurosawa, N. Momono, M. Oda, O. Ivashko, M. v. Zimmermann, M. Janoschek, and J. Chang. Disentangling intertwined quantum states in a prototypical cuprate superconductor. arXiv:2009.06967 2020.

[52] S. A. Kivelson, E. Fradkin, and V. J. Emery. Electronic liquid-crystal phases of a doped Mott insulator. *Nature*, 393:550, 1998.

[53] O. Cyr-Choinière, R. Daou, F. Laliberté, C. Collignon, S. Badoux, D. LeBoeuf, J. Chang, B. J. Ramshaw, D. A. Bonn, W. N. Hardy, R. Liang, J.-Q. Yan, J.-G. Cheng, J.-S. Zhou, J. B. Goodenough, S. Pyon, T. Takayama, H. Takagi, N. Doiron-Leyraud, and Louis Taillefer. Pseudogap temperature T^* of cuprate superconductors from the Nernst effect. *Phys. Rev. B*, 97:064502, Feb 2018.

[54] N. Auvray, B. Loret, S. Benhabib, M. Cazayous, R. D. Zhong, J. Scheeloch, G. D. Gu, A. Forget, D. Colson, Paul. I, A. Sacuto, and Y. Gallais. Nematic fluctuations in the cuprate superconductor $Bi_2Sr_2CaCu_2O_{8+\delta}$. *Nature Communications*, 10(5209), 2019.

[55] S.-H. Baek, A. Erb, and B. Büchner. Low-energy spin dynamics and critical hole concentrations in $la_{2-x}sr_xcuo_4$ ($0.07 \leq x \leq 0.2$) revealed by ^{139}La and ^{63}Cu nuclear magnetic resonance. *Phys. Rev. B*, 96:094519, Sep 2017.

[56] A. Arsenault, S. K. Takahashi, T. Imai, W. He, Y. S. Lee, and M. Fujita. ^{139}La nmr investigation of the charge and spin order in a $la_{1.885}sr_{0.115}cuo_4$ single crystal. *Phys. Rev. B*, 97:064511, Feb 2018.

[57] M.-H. Julien, F. Borsa, P. Carretta, M. Horvatić, C. Berthier, and C. T. Lin. Charge segregation, cluster spin glass, and superconductivity in $la_{1.94}sr_{0.06}cuo_4$. *Phys. Rev. Lett.*, 83:604–607, Jul 1999.

[58] S. Katano, M. Sato, K. Yamada, T. Suzuki, and T. Fukase. Enhancement of static antiferromagnetic correlations by magnetic field in a superconductor $La_{2-x}Sr_xCuO_4$ with $x = 0.12$. *Phys. Rev. B*, 62:R14677–R14680, 2000.

[59] A. T. Savici, A. Fukaya, I. M. Gat-Malureanu, T. Ito, P. L. Russo, Y. J. Uemura, C. R. Wiebe, P. P. Kyriakou, G. J. MacDougall, M. T. Rovers, G. M. Luke, K. M. Kojima, M. Goto, S. Uchida, R. Kadono, K. Yamada, S. Tajima, T. Masui, H. Eisaki, N. Kaneko, M. Greven, and G. D. Gu. Muon spin relaxation studies of magnetic-field-induced effects in high-T_c superconductors. *Phys. Rev. Lett.*, 95:157001, Oct 2005.

[60] B. Khaykovich, S. Wakimoto, R. J. Birgeneau, M. A. Kastner, Y. S. Lee, P. Smeibidl, P. Vorderwisch, and K. Yamada. Field-induced transition between magnetically disordered and ordered phases in underdoped $la_{2-x}sr_xCuo_4$. *Phys. Rev. B*, 71:220508, Jun 2005.

[61] J. Chang, A. P. Schnyder, R. Gilardi, H. M. Rønnow, S. Pailhes, N. B. Christensen, Ch. Niedermayer, D. F. McMorrow, A. Hiess, A. Stunault, M. Enderle, B. Lake, O. Sobolev, N. Momono, M. Oda, M. Ido, C. Mudry, and J. Mesot. Magnetic-field-induced spin excitations and renormalized spin gap of the underdoped $La_{1.895}Sr_{0.105}CuO_4$ superconductor. *Phys. Rev. Lett.*, 98:077004, Feb 2007.

[62] G. S. Boebinger, Yoichi Ando, A. Passner, T. Kimura,

M. Okuya, J. Shimoyama, K. Kishio, K. Tamasaku, N. Ichikawa, and S. Uchida. Insulator-to-metal crossover in the normal state of $La_{2-x}Sr_xCuO_4$ near optimum doping. *Phys. Rev. Lett.*, 77:5417–5420, Dec 1996.

[63] D. R. Harshman, G. Aeppli, G. P. Espinosa, A. S. Cooper, J. P. Remeika, E. J. Ansaldo, T. M. Riseman, D. Ll. Williams, D. R. Noakes, B. Ellman, and T. F. Rosenbaum. Freezing of spin and charge in $la_{2-x}sr_xCuo_4$. *Phys. Rev. B*, 38:852–855, Jul 1988.

[64] S. M. Hayden, G. Aeppli, H. Mook, D. Rytz, M. F. Hundley, and Z. Fisk. Magnetic fluctuations in $la_{1.95}ba_{0.05}cuo_4$. *Phys. Rev. Lett.*, 66:821–824, Feb 1991.

[65] Isao Watanabe, Tadashi Adachi, Satoshi Yairi, Yoji Koike, and Kanetada Nagamine. Change of the dynamics of internal fields in the normal state of la2-xsrxcuo4 observed by muon-spin-relaxation. *Journal of the Physical Society of Japan*, 77(12):124716, 2008.

[66] X. F. Sun, Seiki Komiya, J. Takeya, and Yoichi Ando. Magnetic-field-induced localization of quasiparticles in underdoped $la_{2-x}sr_xcuo_4$ single crystals. *Phys. Rev. Lett.*, 90:117004, Mar 2003.

[67] P. Bourgeois-Hope, S. Y. Li, F. Laliberté, S. Badoux, S. M. Hayden, N. Momono, T. Kurosawa, K. Yamada, H. Takagi, Nicolas Doiron-Leyraud, and Louis Taillefer. Link between magnetism and resistivity upturn in cuprates: a thermal conductivity study of $La_{2-x}Sr_xCuO_4$. arXiv:1910.08126 2019.

[68] T. Fukase, T. Hanaguri, T. Nomoto, T. Goto, Y. Koike, Shinohara T., T. Sato, I. Tanaka, and H. Kojima. Ultrasonic and NQR studies of structural phase transitions and superconductivity in $La_{2-x}Sr_xCuO_4$. *JJAP series*, 7:213–218, 1992.

[69] F. Cordero, A. Paolone, R. Cantelli, and M. Ferretti. Anelastic spectroscopy of the cluster spin-glass phase in $La_{2-x}Sr_xCuO_4$. *Phys. Rev. B*, 62:5309–5312, Sep 2000.

[70] J. Chang, J. S. White, M. Laver, C. J. Bowell, S. P. Brown, A. T. Holmes, L. Maechler, S. Strässle, R. Gilardi, S. Gerber, T. Kurosawa, N. Momono, M. Oda, M. Ido, O. J. Lipscombe, S. M. Hayden, C. D. Dewhurst, R. Vavrin, J. Gavilano, J. Kohlbrecher, E. M. Forgan, and J. Mesot. Spin density wave induced disordering of the vortex lattice in superconducting $La_{2-x}Sr_xCuO_4$. *Phys. Rev. B*, 85:134520, Apr 2012.

[71] T. Goto, T. Suzuki, K. Chiba, T. Shinoda, M. Mori, and T. Fukase. Field-induced spin reorientation and low-temperature structural phase transition in $La_{2-x}Sr_xCuO_4$. *Physica B: Condensed Matter*, 246-247:572 – 575, 1998.

[72] Y. Koyama, Y. Wakabayashi, K. Ito, and Y. Inoue. Low-temperature structural transitions and T_c suppression in $La_{2-x}M_xCuO_4$ (M=Ba, Sr). *Phys. Rev. B*, 51:9045–9051, Apr 1995.

[73] Y. Horibe, Y. Inoue, and Y. Koyama. Direct observation of dynamic local structure in $La_{2-x}Sr_xCuO_4$ around $x = 0.12$. *Phys. Rev. B*, 61:11922–11927, May 2000.

[74] F. Cordero, A. Paolone, R. Cantelli, and M. Ferretti. Pinning of the domain walls of the cluster spin-glass phase in the low-temperature-tetragonal phase of $La_{2-x}Ba_xCuO_4$. *Phys. Rev. B*, 64:132501, Aug 2001.

Appendix A: Vortex lattice contribution to the ultrasound properties

In our experiments with $B \parallel [001]$, the c_{11} acoustic mode probes the compression modulus of the vortex lattice (VL), whereas $(c_{11}-c_{12})/2$ probes its shear modulus. The latter is notorious for its small value, beyond our resolution. On the other hand the compression modulus of the VL should make a detectable contribution. This contribution should give a step-like increase of the sound velocity and an attenuation peak when decreasing temperature through the depinning transition of the vortex lattice. Both these features should move to lower temperatures with increasing field and disappear for $B \geq B_{c2}$.

In Fig. 2(a, b) there is no evidence of the vortex lattice depinning transition. It has a negligible contribution to the longitudinal sound velocity in LSCO $p = 0.12$. This is due to the low value of the irreversibility field, and presumably also because of the two-dimensional and disordered character of the VL at this doping level [70]. Consequently no signature of the vortex lattice depinning transition is observed in Fig. 2(a, b) and Fig. 3.

Appendix B: Impact of superconductivity on the ultrasound properties

We discuss the effect of superconductivity on the ultrasound properties which is best observed at low fields. Below 5 T or so, $T_{\min}$ coincides with T_c in both c_{11} and $(c_{11} - c_{12})/2$ in our LSCO $p = 0.12$ sample (see Fig. 1 and Fig. 2). This behaviour has also been observed in LSCO $p \approx 0.14$ up to 14 T by Nohara and coworkers [12]. In this field range $T_{\min}$ appears to be primarily set by superconductivity.

In LSCO, superconductivity can induce an increase of the sound velocity for $T < T_c$ via two mechanisms. First, the superconducting order parameter has a direct coupling with the lattice for $T < T_c$. In cuprates, this coupling produces a hardening in the superconducting state, for both longitudinal and transverse modes [21]. Consequently, an upturn can occur at T_c in both $(c_{11} - c_{12})/2$ and c_{11}. The second possible mechanism is indirect, and involves the competition between superconductivity and magnetism. In zero and low field, the growth of the magnetic susceptibility $\chi_4(\omega = 0, T)$, signaled by the softening of the sound velocity, can be tempered by the onset of superconductivity. If $\chi_4(\omega = 0, T)$ is sufficiently modified through T_c, it can result in an upturn at T_c. As a result of these two possible mechanisms, at zero and low magnetic field, we observe $T_{\min} = T_c$, and $T_{\min}$ decreases as field increases.

However, for $B \geq 5$ T, $T_{\min}$ increases with magnetic field, meaning that the mechanism causing the softening for $T > T_{\min}$ and the hardening for $T < T_{\min}$ observed for $B \geq 5$ T in LSCO $p = 0.12$ does not involve the coupling of the superconducting order parameter to the lattice. Increasing the magnetic field above $B = 14$ T

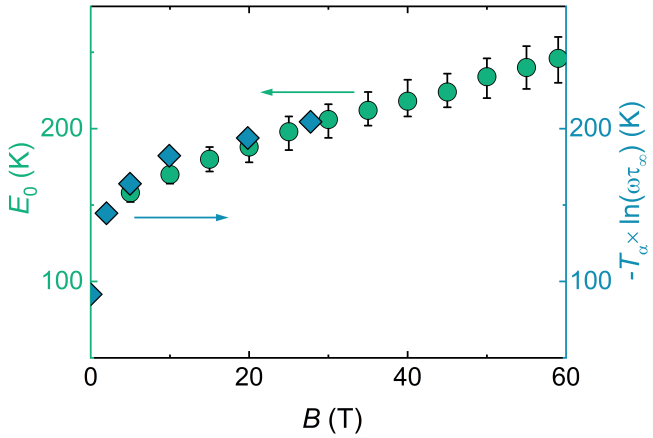

Figure B.1: Comparison between the E_0 energy scale (circles, left scale) extracted from the fitting procedure of Fig. 5 and $-T_\alpha \times \ln(\omega\tau_\infty)$ (diamonds, right scale) determined directly from the data shown in Fig. 2(b), $\omega = 2\pi \times 110$ MHz and $\tau_\infty \approx 10^{-13}$ s. The energy scale $-T_\alpha \times \ln(\omega\tau_\infty)$ corresponds to an experimental determination of E_0 solely based on T_α, using the condition $\omega\tau_4(T_\alpha) = 1$ in Eq. 6 (see text). The rapid drop of $-T_\alpha \times \ln(\omega\tau_\infty)$ at low B is most likely due to the impact of superconductivity on the spin dynamics. Error bars on this quantity are smaller than the size of the symbols.

at $p \approx 0.14$ leads to the same observation [18]. As field increases the superconducting contribution to the sound velocity becomes weaker and the spin freezing contribution larger. For $B \geq 5$ T the superconducting contribution is dwarfed by the contribution from the magnetic slowing down. This explains why the difference between $T_{\min}$ and $T_\alpha = T_{\rm f}$ is large and strongly field dependent for $B < 5$ T, while smaller and constant for higher fields (see Fig. 2(c)).

The temperature scale T_α is insensitive of a direct contribution from superconductivity. While in conventional superconductors, the opening of the superconducting gap causes an attenuation drop, there is no corresponding behaviour in LSCO $p \approx 0.12$. However $\Delta\alpha(T)$ can be indirectly impacted by the onset of superconductivity at low field because the latter modifies the spin dynamics that controls $\Delta\alpha(T)$. This is best illustrated by the zero field $\Delta\alpha(T)$ that shows a remarkable kink at T_c and then a maximum at $T_\alpha \simeq 9.5$ K (see Fig. 2(b)). Within the dynamical susceptibility model, the ultrasound attenuation is mostly governed by the energy scale E_0 entering τ_4 as indicated by Eq. 4. The kink anomaly at $T_{\rm c}$ in $\Delta\alpha(T)$ in zero field can be interpreted as a decrease of E_0 for $T < T_{\rm c}$ caused by the onset of superconductivity.

Because the dynamical susceptibility model does not take into account the impact of superconductivity on spin dynamics, we use an alternative scheme in order to extract E_0 for $B < 5$ T. At $T = T_\alpha$, the condition $\omega\tau_4(T) = 1$ is met. Solving Eq. 6 for E_0 at $T = T_\alpha$ hence yields $E_0 = -T_\alpha/\ln(\omega\tau_\infty)$ [38]. In Fig. B.1 we compare this T_α derived E_0 with E_0 of Fig. 5(c) obtained with the parametrization of the ultrasound data. Good agreement is found between the two estimations of E_0. As seen in Fig. B.1, $-T_\alpha/\ln(\omega\tau_\infty)$ decreases rapidly at low fields, dropping from $E_0 \sim 150K$ for $B = 5$ T to $E_0 = 92$ K for $B = 0$. This rapid drop reflects the competition between spin freezing and superconductivity.

Appendix C: Previous experiments on polycrystals

In section V B we discuss a scenario that would explain the lattice hardening seen mainly in the c_{11} elastic constant at low temperature. Here, we detail previous putative explanations that have been proposed to explain a similar phenomenology from ultrasound and anelastic studies of polycrystalline La-based compounds.

We first consider previous ultrasound experiments. Around $p \approx 0.12$, in several La-based cuprates and in particular LSCO [13, 14, 68, 71], the sound velocity of longitudinal waves increases markedly at low temperature while an attenuation peak occurs. This behaviour is most likely related to the anomalous hardening of the c_{11} elastic constant, as suggested by the similar temperature scales and field-enhancement. Interestingly, those previous ultrasound studies have shown that the temperature scale of the lattice hardening evolves smoothly from LBCO $p = 0.12$ to LSCO $p = 0.12$, and correspond to the coincident OMT-LTT and charge-stripe transition in the former [13, 68]. Based on these experiments it has been proposed that in LSCO $p \approx 0.12$ the low temperature lattice hardening arises from the parallel development of local and/or fluctuating LTT distorsions and charge-stripes. However, in this scenario it is unclear why the lattice hardening is observed only at low temperature - comparable to T_α - whereas, in LSCO $p \approx 0.12$, LTT-type tilts are found at temperatures as high as $T = 100$ K in electron diffraction experiments [72, 73] and LTT-type reflections are observed up to the OMT-HTT transition temperature $T_{\rm st}$ in X-Ray diffraction [7].

Now let us consider anelastic experiments in LSCO and LBCO polycrystals. These have shown that the Young modulus increases markedly at low temperature [74]. The elastic energy loss coefficient shows a step-like increase for $T \leq T_{\rm f}$ and a plateau down to the lowest T [69]. Based on a comparison with nuclear quadrupolar resonance (NQR) experiment, as well as the effect of oxygen vacancy, it has been inferred that the anelastic anomalies arise from a strain induced motion of the antiferromagnetic domain walls of the AFM glass phase [69]. In particular this naturally explains why these anomalies are observed at temperatures of the order of T_α. However, these experiments are performed at much lower frequency than the ultrasound ones (within the kHz range) and thus don't necessarily probe the same relaxation process as ultrasound experiments [36].